Ann. Geophys., 30, 797–809, 2012
www.ann-geophys.net/30/797/2012/
doi:10.5194/angeo-30-797-2012

Annales Geophysicae

A new global model for the ionospheric F2 peak height for radio wave propagation

M. M. Hoque and N. Jakowski

Institute of Communications and Navigation, German Aerospace Center, Neustrelitz, Germany

Correspondence to: M. M. Hoque (mainul.hoque@dlr.de)

Received: 30 November 2011 – Revised: 23 February 2012 – Accepted: 4 April 2012 – Published: 7 May 2012

Abstract. The F2-layer peak density height *hm*F2 is one of the most important ionospheric parameters characterizing HF propagation conditions. Therefore, the ability to model and predict the spatial and temporal variations of the peak electron density height is of great use for both ionospheric research and radio frequency planning and operation. For global *hm*F2 modelling we present a nonlinear model approach with 13 model coefficients and a few empirically fixed parameters. The model approach describes the temporal and spatial dependencies of *hm*F2 on global scale. For determining the 13 model coefficients, we apply this model approach to a large quantity of global *hm*F2 observational data obtained from GNSS radio occultation measurements onboard CHAMP, GRACE and COSMIC satellites and data from 69 worldwide ionosonde stations. We have found that the model fits to these input data with the same root mean squared (RMS) and standard deviations of 10 %. In comparison with the electron density NeQuick model, the proposed Neustrelitz global *hm*F2 model (Neustrelitz Peak Height Model – NPHM) shows percentage RMS deviations of about 13 % and 12 % from the observational data during high and low solar activity conditions, respectively, whereas the corresponding deviations for the NeQuick model are found 18 % and 16 %, respectively.

Keywords. Ionosphere (Modelling and forecasting)

1 Introduction

The ionospheric F2-layer is primarily responsible for the reflection of high frequency (HF) radio waves in the ionosphere. Thus, the F2-layer peak density height *hm*F2 is one of the most important parameters needed for radio frequency planning and spectrum management. The regular variation of the solar radiation with the solar zenith angle causes temporal and spatial variations of *hm*F2. Depending on the solar activity, daytime and season, the peak density height may range from 350 to 500 km at equatorial latitudes and from 250 to 350 km at mid-latitudes. Additionally, there is a strong dependency of *hm*F2 on dynamic forces such as electric fields and neutral winds. Due to regular and irregular variations of the bottomside plasma density closely related to the *Nm*F2 and *hm*F2 variations, the terrestrial signal transmission may be interrupted or even lost; moreover, the transmission coverage may be affected due to up or down lifting of the ionospheric plasma, changing the *hm*F2 height.

Furthermore, the Earth-space transionospheric communication can also benefit from the knowledge of the *hm*F2 and *Nm*F2. As an example, GNSS (global navigation satellite system) positioning can be improved by mitigating higher order ionospheric propagation effects such as ray path bending errors using *Nm*F2 and *hm*F2 information (see Hoque and Jakowski, 2008, 2011a). Again, since F2-layer peak is a key anchor point to construct ionospheric electron density profiles, *Nm*F2 and corresponding *hm*F2 are the most important parameters in empirical ionospheric modelling. The accuracy of the peak height is crucial in some other applications too, such as inferring the neutral wind (e.g. Zhang et al., 2003).

To develop *hm*F2 prediction model, early work was done by Shimazaki (1955), Bradley and Dudeney (1973), Bilitza et al. (1979), and Dudeney (1983) utilizing the propagation factor M(3000)F2. The M(3000)F2 can be deduced from vertical-incidence ionograms using standard methods (Piggott and Rawer, 1972, 1978). The propagation factor M(3000)F2 is related to the maximum usable frequency MUF(3000) by M(3000)F2 = MUF(3000)/*fo*F2, where MUF(3000) is defined as the highest frequency at which a radio wave can be received over a distance of

3000 km after reflection in the ionosphere (Bradley and Dudeney, 1973). Shimazaki (1955) found that *hm*F2 is inversely related to M(3000)F2. Bradley and Dudeney (1973), Bilitza et al. (1979), and Dudeney (1983) obtained better results after considering dependency of *hm*F2 on the ratio of critical frequencies in the F2 and E layer *fo*F2/*fo*E, sunspot number and geomagnetic latitude, in addition to its dependency on the M(3000)F2. In another approach, McNamara et al. (1987), Kishcha and Kochenova (1996) computed *hm*F2 directly from ionosonde measurements using true height analysis.

Similar work was done by Jones and Obitts (1970), Rush et al. (1983, 1984), Fox and McNamara (1988), Bilitza et al. (1990), Bilitza (2001), and Bilitza and Reinisch (2008) in developing global ionospheric parameter models. Considering the importance of ionospheric characteristics in radio frequency planning, the International Telecommunications Union (ITU) issued a standard set of ionospheric parameter models (CCIR, 1967; ITU-R, 1997) on advice from its International Radio Consultative Committee (CCIR), presently from its Radio-Communication Sector (ITU-R). The CCIR models and related software are available via ITU. The CCIR model consists of 24 maps, each one containing 441 coefficients for one month of the year and one of the two levels of solar activity, R12 = 10 and 100, where R12 is the 12-month running mean of the monthly sunspot number (1764 coefficients in all) (Jones and Gallet, 1962, 1965). Many empirical models such as the International Reference Ionosphere (IRI) model (Bilitza and Reinisch, 2008), the NeQuick model (Radicella and Leitinger, 2001; Coisson et al., 2006; Nava et al., 2008) and even some theoretical models use the CCIR maps for *fo*F2 and *hm*F2 estimations. The IRI model uses modified Bilitza et al. (1979) equations for *hm*F2 estimation in any place and time using CCIR maps.

A new approach for global ionospheric parameters prediction based on neural network (NN) technique is studied by Altinay et al. (1997), Wintoft and Cander (1999), Kumluca et al. (1999), Tulunay et al. (2000), McKinnell and Poole (2001), Poole and Poole (2002), Oyeyemi and Poole (2004), and Oyeyemi et al. (2005). Xenos (2002) demonstrated the NN technique for single station modelling and regional mapping of M(3000)F2 in the European region.

Another approach of ionospheric parameter modelling based on empirical orthogonal function (EOF) analysis of the observational data set is studied by Liu et al. (2008), and Zhang et al. (2009). Furthermore, Gulyaeva et al. (2008) recently developed a numerical model of *hm*F2 using about 90 000 electron density profiles derived from observations taken by topside sounder satellites ISIS1, ISIS2, IK19 and Cosmos-1809 during 1969–1987.

In this paper, we derive an empirical *hm*F2 model based on non-linear least squares technique. For this, we considered a set of nonlinear equations with 13 polynomial coefficients describing the regular variations of the peak density height. The polynomial coefficients are derived from a nonlinear fit with *hm*F2 measurements in least squares sense. For this, we used two types of measurement data, namely space-based GNSS ionospheric radio occultation (IRO) measurements and ground-based ionosonde observations. CHAMP (CHAllenging Minisatellite Payload) IRO data are used for inputs under both solar maximum and minimum conditions (2001–2008), whereas GRACE (Gravity Recovery And Climate Experiment) and COSMIC (Constellation Observing System for Meteorology, Ionosphere and Climate, also known as FORMOSAT-3) IRO data are used for the low solar activity period 2006–2010. Additionally, we used a large database of propagation factors M(3000)F2 and *hm*F2, collected through a worldwide network of 69 ground ionosondes over the last 60 years.

2 Data sources

The most powerful source of *hm*F2 data used in the present study is the IRO observation. We used *hm*F2 estimates reconstructed from IRO measurements onboard CHAMP, GRACE and COSMIC satellite missions. We used about 300 000 CHAMP retrievals covering high, medium and low solar activity periods from April 2001 to August 2008. About 60 000 GRACE retrievals were used within the time period of April 2008 to December 2010. The IRO data from CHAMP and GRACE are processed by the German Aerospace Center (DLR) Neustrelitz and available at http://swaciweb.dlr.de/ for registered users. Additionally, we used about 2.5 millions *hm*F2 estimates reconstructed from COSMIC IRO observation. The COSMIC IRO data are routinely processed by the COSMIC Data Analysis and Archive Center (CDAAC) and available at http://cosmic-io.cosmic.ucar.edu/cdaac/index.html.

The IRO technique allows all-day all-season monitoring of the Earth's atmosphere (Hajj and Romans, 1998; Jakowski et al., 2002). Typical polar orbits of the LEO satellites together with the daily rotation of the Earth extend the data coverage over the globe. Thus, IRO data include day and night, summer, winter and equinoxes at high, medium and low latitudes. In general, the retrieved *Nm*F2 and *hm*F2 by IRO techniques are in good agreement with ionosonde observations at medium latitudes (Jakowski et al., 2004; Angling, 2008). However, the accuracy of the reconstructed electron density profiles may degrade as a consequence of strong spatial gradients in the ionosphere, especially in the equatorial anomaly regions (Yue et al., 2010).

A large number of ionosonde data from three different sources, namely Space Physics Interactive Data Resource (SPIDR), Ionosphere Prediction Service (IPS), and National Oceanic and Atmospheric Administration (NOAA) was used in the present study. The National Geophysical Data Center (NGDC) of the United States of America (USA) provides historical and present ionosonde data records such as *fo*F2, *hm*F2, *fo*E etc. to the scientific community via SPIDR.

The SPIDR database (available at http://spidr.ngdc.noaa.gov/spidr/) currently contains over 60 years of ionospheric data from over 200 ionosondes worldwide. However, we found that for many stations *hm*F2 data are completely missing and for some stations data are available only for short periods.

Using the available data we computed long-time median and mean of the solar cycle variation, annual-semiannual variation and diurnal variation of *hm*F2 for individual stations. In some cases the median and mean variations do not follow the same pattern or largely deviate from the typical diurnal pattern, such as high *hm*F2 values during nighttime, sharp decrease in morning hours and gradual increase during daytime. In such cases the station is excluded from the database. Finally, we are able to use data from only 37 ionosonde stations from SPIDR. We sorted *hm*F2 data for selected stations and used medians for further processing of the data.

The IPS Australia is another source of historical ionospheric data used in this study (available at ftp://ftp.ips.gov.au/wdc-data/iondata/au/). The IPS stations are well-distributed over Australia. The IPS does not provide *hm*F2. Instead, it provides the propagation factor M(3000)F2. We used M(3000)F2 from 27 ionosonde stations provided by the IPS. Different techniques for estimating *hm*F2 from M(3000)F2 are reviewed in Dudeney (1983). However, we follow the algorithm/approach used in the NeQuick model, which was originally given by Radicella and Zhang (1995) based on the Dudeney (1978, 1983) formula. For readers of this paper, we include the algorithm in the following:

$$hmF2 = \frac{1490MF}{M + \Delta M} - 176, \quad (1)$$

in which

$$\Delta M = \begin{cases} \frac{0.253}{foF2/foE - 1.215} - 0.012 \\ -0.012 \quad \text{if} \quad foE = 0 \end{cases}, \quad (2)$$

$$MF = M\sqrt{\frac{0.0196M^2 + 1}{1.2967M^2 - 1}}. \quad (3)$$

In Eq. (1), *hm*F2 is in km where $M = $ M(3000)F2 and *fo*F2 is the critical ionosonde frequency related to the peak electron density by $NmF2 = 1.24 \times 10^{-2}(foF2)^2$. The quantity *fo*E is the critical frequency of the ionospheric E layer. Like the NeQuick model, for computing *fo*E we follow the Titheridge model (Leitinger et al., 1995; Titheridge, 1996), which is based on the seasonal relationship of *fo*E with the solar radio flux F10.7 and solar zenith angle χ.

$$(foE)^2 = a_e\sqrt{F10.7}\,(\cos\chi_{\text{eff}})^{0.6} \quad (4)$$

where a_e is a seasonal term and its values are given in Nava et al. (2008) and χ_{eff} is the effective solar zenith angle defined by

$$\chi_{\text{eff}} = \chi \quad \text{when} \quad \chi \le 86.23^\circ, \quad (5)$$

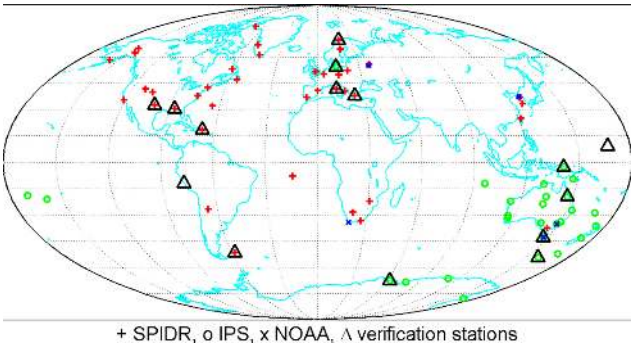

Fig. 1. Global map of used ionosonde stations including 15 verification stations.

$$\chi_{\text{eff}} = 90^\circ - 0.24^\circ \exp\left(20^\circ - 0.2\chi\right) \text{ when } \chi > 86.23^\circ. \quad (6)$$

Using Eqs. (1)–(6) we converted M(3000)F2 to corresponding *hm*F2 values. Then, we computed the solar cycle variation, annual-semiannual variation and daily variation of *hm*F2 for individual stations. Depending on the mean and median analysis of *hm*F2 variation, we excluded stations for which the median and mean variations largely deviate from each other. Additionally, we used M(3000)F2 data from five ionosonde stations provided by NOAA via archives at ftp://ftp.ngdc.noaa.gov/ionosonde/data/. As before, we converted M(3000)F2 to corresponding *hm*F2 values using Eqs. (1)–(6) and checked them before using in further processing. To view the ionosonde data coverage, a global map of used ionosonde stations from SPIDR, IPS and NOAA sources is given in Fig. 1. Fifteen verification stations that were used for validation purposes are also indicated in the map.

We arranged a large *hm*F2 database, bringing together IRO data and ionosonde data. The database includes different combinations of data, like day and night, summer, winter and equinoxes, high, medium and low solar and geomagnetic activity conditions, and high, medium and low geographic/geomagnetic latitudes. After completion, we sorted and thus minimized the database to reduce the computational complexity in the fitting procedures. We sorted the database with respect to F10.7 variation, seasonal variation (i.e. day of year), local time variation and geomagnetic latitude and longitude variations. To consider the seasonal variation, *hm*F2 values were averaged for 27 day-intervals and the 14th day was taken as the reference day. The spatial resolution in the meridional direction was limited to 2.5°. In the zonal direction, the maximum spatial resolution was 5° at the equator and the resolution was gradually decreased to 360° at the poles. The local time resolution was limited to 1 h. Thus, the length of the input data matrix was reduced to about 1 million values.

3 Modelling approach

In our recent papers (Jakowski et al., 2011a, b; Hoque and Jakowski, 2011b), we developed basic approaches for modelling ionospheric parameters on global scale, e.g. NTCM (Neustrelitz TeC Model) and NPDM (Neustrelitz Peak Density Model) approaches. Following the same basic approach, in the present work we developed a set of nonlinear equations describing the dependencies of *hm*F2 on local time, season, geomagnetic field and solar activity as

$$hmF2 = F_1 F_2 F_3 F_4 \tag{7}$$

where the factors F_{1-4} contain explicitly the model functions including model coefficients that describe four main dependencies of *hm*F2. The factor F_1 describes the daily variation with local time (LT in hours) as

$$\begin{aligned} F_1 =& 1 + c_1 \cos\chi^{**} \\ &+ \begin{pmatrix} c_2\cos(V_D) + c_3\sin(V_D) + c_4\cos(V_{SD}) \\ + c_5\sin(V_{SD}) + c_6\cos(V_{TD}) + c_7\sin(V_{TD}) \end{pmatrix} \cos\chi^{*} \end{aligned} \tag{8}$$

$$V_D = \frac{2\pi\,\mathrm{LT}}{24}, \quad V_{SD} = \frac{2\pi\,\mathrm{LT}}{12}, \quad V_{TD} = \frac{2\pi\,\mathrm{LT}}{8} \tag{9}$$

where V_D, V_{SD} and V_{TD} are the angular phases of the diurnal, semi-diurnal and terdiurnal harmonic components, respectively. The functions $\cos\chi^*$ and $\cos\chi^{**}$ describe the dependency on the solar zenith angle χ as

$$\cos\chi^{*} = \sin\varphi\sin\delta + \cos\varphi\cos\delta - \frac{2\varphi}{\pi}\sin\delta \tag{10}$$

$$\cos\chi^{**} = \sin\varphi\sin\delta + \cos\varphi\cos\delta + P_{F1} \tag{11}$$

where ϕ is the geographic latitude and δ is the declination of the sun. The value $P_{F1} = 0.4$ in Eq. (11) is chosen in such a way that the term $\cos\chi^{**}$ has always a positive contribution. The factor F_2 describes the annual (A) and the semi-annual (SA) variation of *hm*F2 as given by Eq. (12):

$$F_2 = 1 + c_8\cos(V_A) + c_9\cos(V_{SA}), \tag{12}$$

in which

$$V_A = 2\pi\,\frac{(\mathrm{doy} - \mathrm{doy_A})}{365.25}, \quad V_{SA} = 4\pi\,\frac{(\mathrm{doy} - \mathrm{doy_{SA}})}{365.25}. \tag{13}$$

The phase shifts are best fitted as $\mathrm{doy_A} = 181$ days and $\mathrm{doy_{SA}} = 49$ days for the annual and the semi-annual variation, respectively.

There is a geomagnetic control over the structure of the peak electron density and its height. Therefore, the peak height depends on the geomagnetic latitude ϕ_m. For simplicity, we used a simple dipole representation of the Earth's magnetic field instead of using any multi-pole representation, such as the International Geomagnetic Reference Field (IGRF) model (Mandea and Macmillan, 2000). The latitudinal distribution of *hm*F2 shows a maximum at the geomagnetic equator, gradually decreasing on both sides of the equator. Our investigation shows that the peak over the geomagnetic equator is prominent during daytime, but becomes weaker during nighttime. Considering this, we modelled latitudinal distribution of *hm*F2 in connection with the local time variation in such a way that the magnitude of *hm*F2 peak is maximum at 14:00 LT and minimum during nighttime. Thus, the latitudinal distribution of *hm*F2 is modelled by the following expression:

$$\begin{aligned} F_3 =& 1 + c_{10}\exp\left(-\frac{\varphi_m^2}{2\sigma_{\varphi 1}^2}\right) \\ &+ c_{11}\exp\left(-\frac{\varphi_m^2}{2\sigma_{\varphi 2}^2}\right)\exp\left(-\frac{(\mathrm{LT}-14)^2}{2\sigma_{LT}^2}\right). \end{aligned} \tag{14}$$

The half widths of the Gaussian function are best fitted as $\sigma_{\phi 1} = 40°$, $\sigma_{\phi 2} = 20°$ and $\sigma_{LT} = 4$ h.

We have found a strong solar activity dependence of *hm*F2, which is modelled by the following equation:

$$F_4 = c_{12} + c_{13}\exp\left(-\frac{\mathrm{F10.7}}{\delta_{\mathrm{F10.7}}^2}\right) \tag{15}$$

where F10.7 is the solar radio flux commonly measured in flux units (1flux unit $10^{-22}\,\mathrm{W\,m^{-2}\,Hz^{-1}}$) and $\delta_{\mathrm{F10.7}} = 10.8$ flux units.

Equations (7)–(15) explicitly describe the functional dependencies of *hm*F2 on local time, season, geographic and geomagnetic latitudes, and solar cycle variations. The equations contain 13 unknown polynomial coefficients in addition to a few empirically fixed known parameters. In the next section, we derive the polynomial coefficients by applying the model approach to the model database.

4 Modelling results

In the previous section, we formulated a set of nonlinear equations that explicitly contain model functions and coefficients. Now, we consider that the model coefficients and observation data are related through a nonlinear system of equations. Then, by non-linear least square methods, we obtained a set of 13 model coefficients. The coefficients best fit the data in the sense of minimizing the sum of squares of residual errors. To assess the degree of certainty for model coefficients, we computed the approximate covariance matrix. The standard deviations of the individual model coefficients were estimated by taking square roots of the diagonal elements of the covariance matrix. The solution coefficients and their percentage standard deviations are given in Table 1. The estimated standard deviations (STD) confirm

Table 1. Optimal set of model coefficients and their percentage standard deviations.

Coefficients	IRO+ionosonde data		IRO data only
	Optimal values	STD %	Optimal values
c_1	0.09246	0.7	0.10409
c_2	0.19113	0.2	0.18189
c_3	0.02297	1.2	0.01958
c_4	0.05666	0.4	0.06091
c_5	−0.01687	−1.3	−0.02510
c_6	−0.01590	−1.4	−0.01255
c_7	0.01194	1.9	0.01374
c_8	−0.01781	−0.9	−0.01216
c_9	−0.00618	−2.5	−0.00668
c_{10}	−0.14070	−0.5	−0.10836
c_{11}	0.46728	0.2	0.45153
c_{12}	348.66432	0.1	334.01077
c_{13}	−184.15337	−0.2	−172.63000

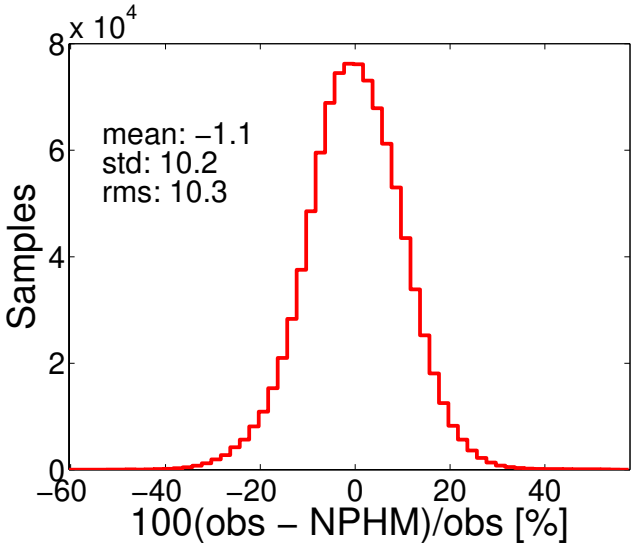

Fig. 2. Histogram of percentage residuals.

that the model coefficients have a large degree of certainty. It should be noted that the coefficients are related to the input data set and they may change if another or additional extended data set is used. The same is true for all the parameters fixed at certain values in the previous section, i.e. they may change when other data sets are used. Additionally, to examine the reliability of the IRO data for ionospheric parameters modelling, we computed the 13 model coefficients using only IRO data in the database. The computed model coefficients are also given in the Table 1. However, the parameters fixed at certain values in the previous section are kept the same. It should be mentioned that all comparisons and validations of NPHM given in this paper are done using coefficients obtained for IRO + ionosonde data. The only exception is Fig. 9 where both sets (IRO + ionosonde and IRO only) of coefficients are used to compare their relative performance and verify the reliability of the IRO data in ionosphere modelling.

To assess the overall fitting quality, we computed model residuals, i.e. the differences between the input data and model values. Then, we computed percentage residuals by (100 × model_residual/input) %. The histogram of percentage residuals is plotted in Fig. 2. The mean deviation, standard deviation (STD) and root mean squared (RMS) estimates of percentage residuals are calculated (see in Fig. 2).

We see that the histogram is normally distributed with a small bias of about −1 % and shows no obvious asymmetric pattern. The RMS and standard deviation are found to be equal with a value of about 10 % each. Some example plots of model results and input data as a function of local time, day of year (doy) and geomagnetic latitude are given in Figs. 3–5. Comparing input data and model values, we see the model accuracy in describing different nonlinear behaviours of the input data.

Figure 3 displays sample plots for the local time variation of *hm*F2 during a summer and a winter day at high, mid and low latitudes at 0° meridian and F10.7 = 80 flux units. We see that the model follows the data trend for most cases. In Fig. 4, the seasonal variations during daytime and nighttime are plotted at mid-latitudes for the same solar activity level. We see that during nighttime the model follows the data trend, whereas during daytime it overestimates *hm*F2 compared to the input data. Figure 5 gives sample plots for the geomagnetic latitude dependency during daytime and nighttime. We see that during daytime the model can successfully follow the input data. During nighttime, it tries to follow the data trend although the data trend is not clear in the input data.

5 Validation

For validation purposes, we did comprehensive test comparisons with observational IRO data and ionosonde data from selected time periods, and also with *hm*F2 estimations from the NeQuick model. It should be noted that the data used for validation purposes are already used as input data sets in the adjustment procedures. However, using a large input database (about 1 million input data sets) we derived only 13 model coefficients; therefore, we assume that it may not be unjustified to use some input data for validation purposes as well.

For comparisons to observational IRO data, we used a large database that includes five years (2002–2006) of CHAMP data and three years (2007–2009) of COSMIC data. The IRO data include data from day and night at high, medium and low latitudes. The data contain a mix of high and low geomagnetic activity conditions. Since we are concerned

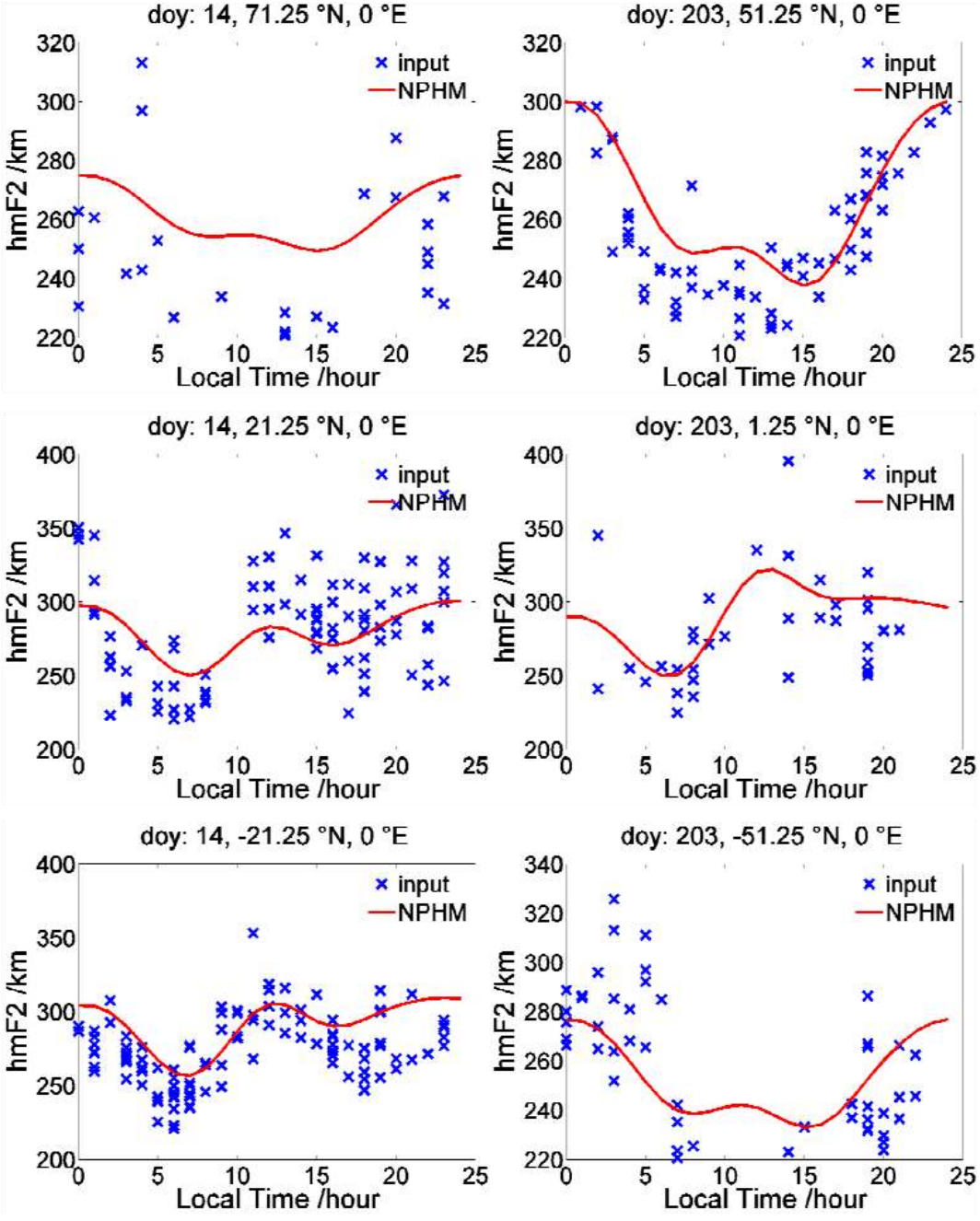

Fig. 3. Local time variation during summer and winter days for day of year 203 and 14 at high, mid and low latitudes: 71.25° N, 51.25° N, 21.25° N, 1.25° N, −21.25° N and −51.25° N at 0° meridian for F10.7 = 80 flux units.

about the ionospheric F2 layer peak height, the observations that exceed the limit 200 km < *hm*F2 < 550 km are excluded from comparisons. The *hm*F2 is calculated by NPHM as well as by NeQuick model at the same location and time window as the IRO data. The percentage residuals are then computed by 100 × (obs − model)/obs % for each year of data and their histograms are shown in Fig. 6.

The corresponding RMS, mean and standard deviation of percentage residuals are given in Fig. 6, and also summarized in Table 2. The table shows that both the NPHM and NeQuick residuals have negative biases for all years considered. Comparing NPHM and NeQuick models, we see that the biases are less for NPHM for all cases. The maximum biases (absolute values) are found −4.8 % and −10.2 % for NPHM and NeQuick model, respectively, during 2009 and the minimum biases are found −0.5 % and −4.4 %, respectively, during 2003. Similarly, the RMS and STD estimates are found less for NPHM in comparisons with the NeQuick

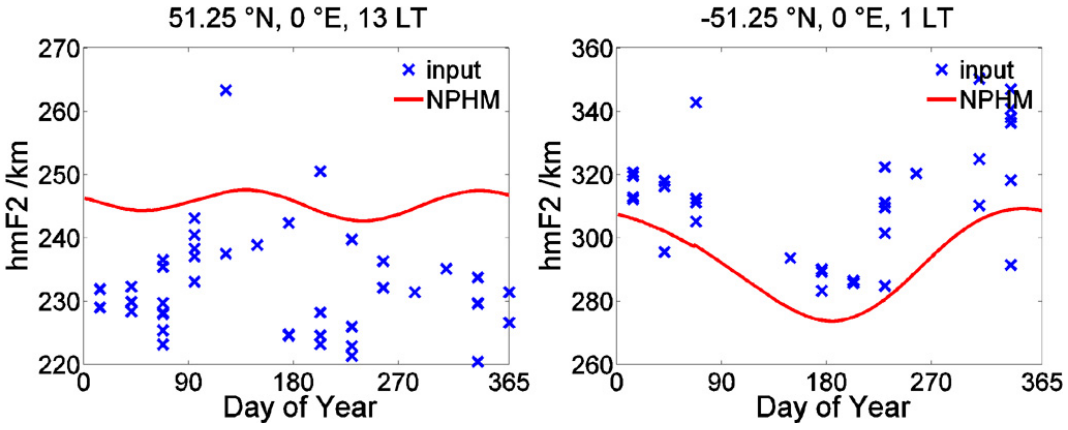

Fig. 4. Seasonal variation at mid-latitudes 51.25° N, −51.25° N at 0° meridian for F10.7 = 80 flux units.

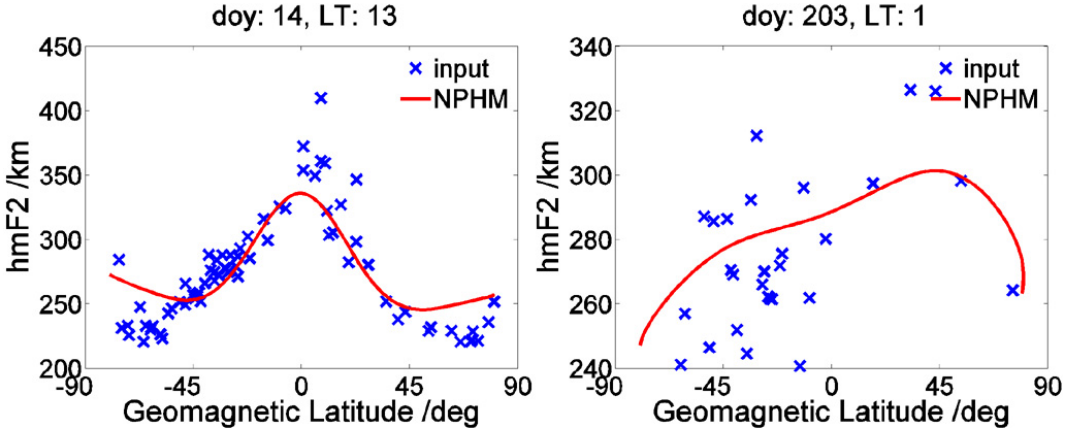

Fig. 5. Geomagnetic latitude variation during summer and winter days for day of year 203 and 14 at 13:00 LT and 01:00 LT for F10.7 = 80 flux units.

model for all years. The maximum STDs are found 13 % and 16.2 % for NPHM and NeQuick models, respectively, during 2002 and the minimum STDs are found 10.9 % and 13.7 %, respectively, during 2009. In general for both models, the RMS and STD of residuals are slightly higher during times of high solar activity compared to those during low solar activity periods. Comparing the statistical estimates given in Table 2, we see that although the NPHM performs slightly better than the NeQuick model, their differences are not much.

For validation with ionosonde data, we chose two one-month periods from high and low solar activity in years 2002 and 2006, respectively. We chose the months May for 2002 and December for 2006; they correspond to the Northern Hemisphere summer and winter, respectively. Depending on the data availability during the specified one-month period, we selected 15 reference ionosonde stations distributed on both sides of the equator at high, medium and low latitudes covering the American, European and Australian longitude sectors.

Due to lack of observational data for the specified one-month period May 2002, we selected May 2001 for Rome and May 2003 for Puerto Rico as the test periods. The station name, location and test period are given in Table 3. Figures 7 and 8 compare the NPHM and NeQuick model results with the ionosonde measurements as a function of Universal Time (UT) at the selected station locations. The *hm*F2 values are averaged at each UT hour for all days in May and December. Figures 7 and 8 show the comparisons to the observational ionosonde data for the Northern and Southern Hemisphere stations, respectively.

Figure 7 shows that NPHM performs better than the NeQuick model at Tromsø, Juliusruh, Rome, Dyess and Puerto Rico during the selected high solar activity month May. Only at Eglin AFB NeQuick performs better than NPHM. During low solar activity period December 2006, NPHM performs better at Dyess, Eglin AFB and Kwajalein, whereas NeQuick performs better at Tromsø, Juliusruh and Athens. Figure 8 shows that at Southern Hemisphere stations Hobart and Macquarie Island, NPHM performs better

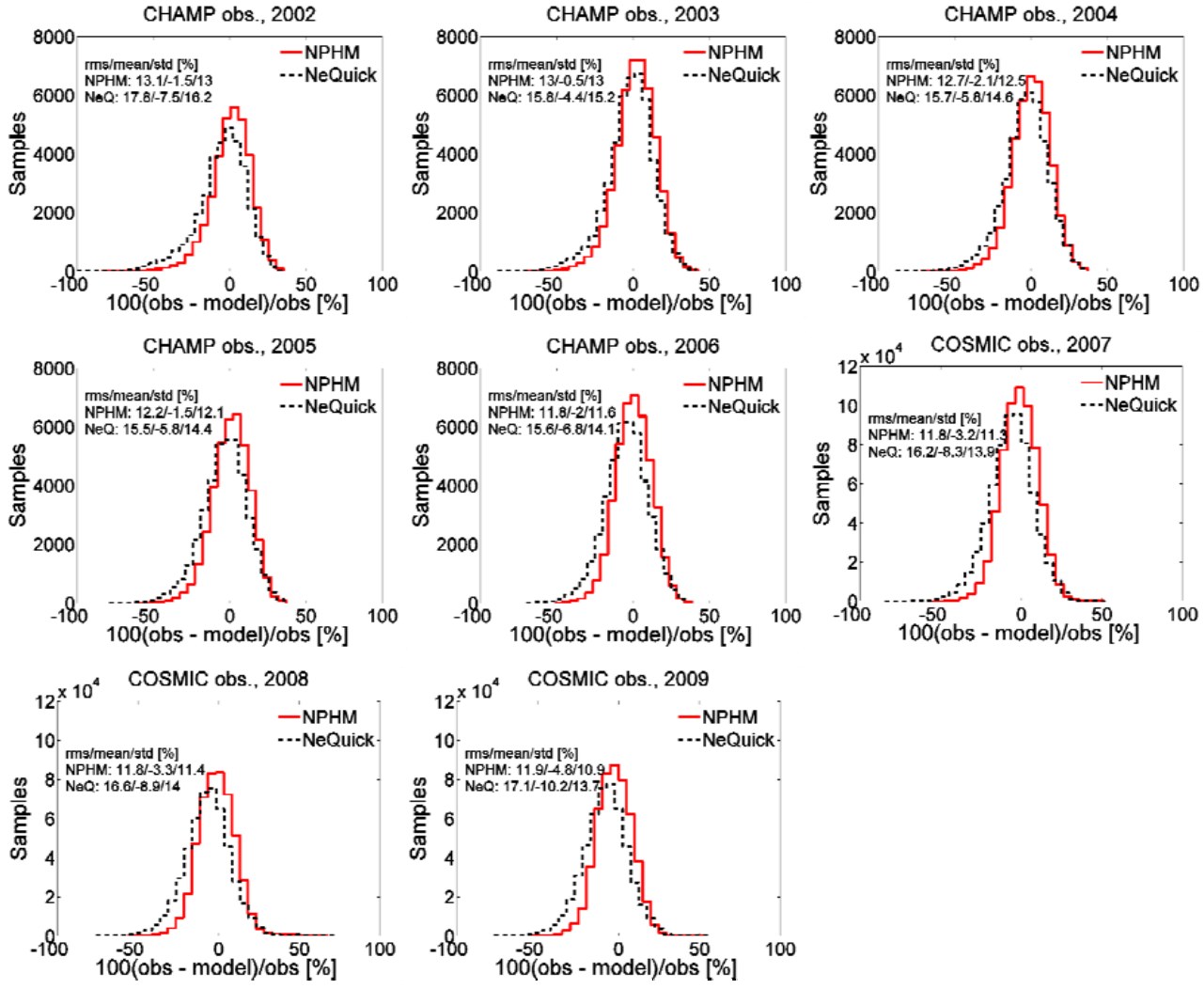

Fig. 6. Percentage histogram of model errors.

Table 2. Estimates of percentage residuals for NPHM and NeQuick model in comparison with IRO data.

Year	Number of obs. used	RMS (%)		Mean (%)		STD (%)	
		NPHM	NeQuick	NPHM	NeQuick	NPHM	NeQuick
2002	33 897	13.1	17.8	−1.5	−7.5	13	16.2
2003	46 389	13	15.8	−0.5	−4.4	13	15.2
2004	41 566	12.7	15.7	−2.1	−5.8	12.5	14.6
2005	39 539	12.2	15.5	−1.5	−5.8	12.1	14.4
2006	42 474	11.8	15.6	−2	−6.8	11.6	14.1
2007	63 3637	11.8	16.2	−3.2	−8.3	11.3	13.9
2008	491 808	11.8	16.6	−3.3	−8.9	11.4	14
2009	500 669	11.9	17.1	−4.8	−10.2	10.9	13.7

than the NeQuick during May 2002. The NeQuick performs better at Vanimo, Townsville and Port Stanley. During December 2006, at Hobart and Mawson NPHM performs better, whereas at Vanimo, Jicamarca and Townswille NeQuick model shows comparatively better performance. Figure 9 also confirms these findings.

As already mentioned, we determined two sets of model coefficients (see Table 1) depending on the used database:

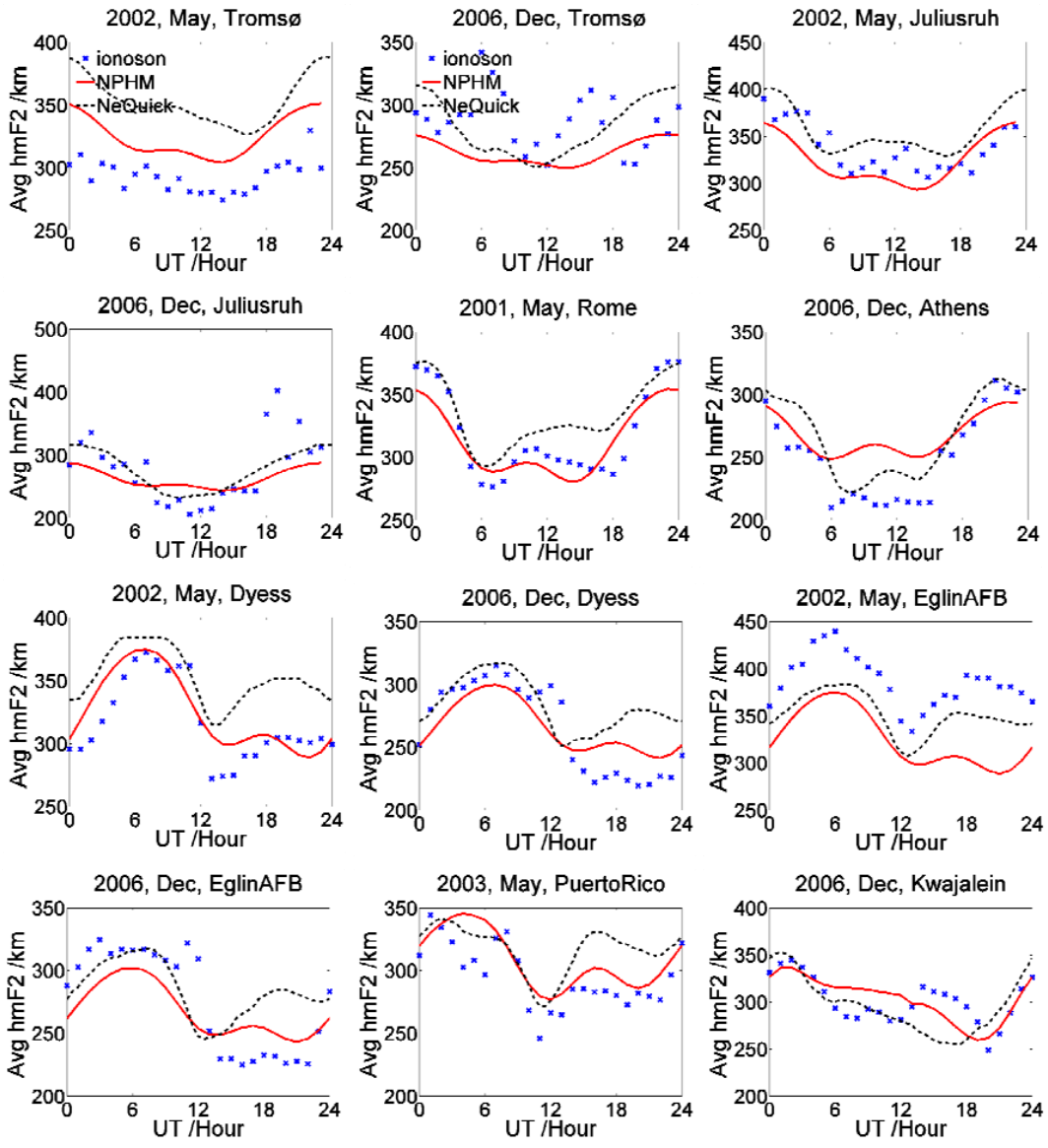

Fig. 7. Monthly mean of NPHM and NeQuick as a function of UT in comparison with ionosonde observation at Northern Hemisphere stations.

IRO + ionosonde or IRO only. For both sets of model coefficients, the RMS estimates of hourly model residuals (obs − model) are computed at each verification station for the selected two one-month periods and their bar charts are shown in Fig. 9. Comparing the bar plots of IRO + ionosonde and IRO only, we see no significant difference in the model performance; that means the IRO data alone can be used for ionosphere parameters modelling.

Comparing bar plots in Fig. 9, we see that although NPHM performs comparatively better than NeQuick model in the Northern Hemisphere, their differences are not much, except at Tromsø and Eglin AFB during May 2002. In the Southern Hemisphere, NeQuick model performs comparatively better for both periods. The NPHM and NeQuick model show their worst performances at Vanimo and Jicamarca, respectively, during December 2006.

Our comparisons show that the NPHM and NeQuick results are comparable, although in terms of number of coefficients, the NPHM model is much simpler than the NeQuick model. To compute *hm*F2 the NeQuick model uses the ITU recommended CCIR (1967) model for *fo*F2 and M(3000)F2, whose coefficients are derived from worldwide ionosonde observations. The CCIR model uses two sets of 24 files, each file in one set containing 998 coefficients and in the other set 441 coefficients for *fo*F2 and M(3000)F2 mapping, respectively. The proposed NPHM needs only 13 coefficients and a few empirically fixed parameters for global *hm*F2 mapping.

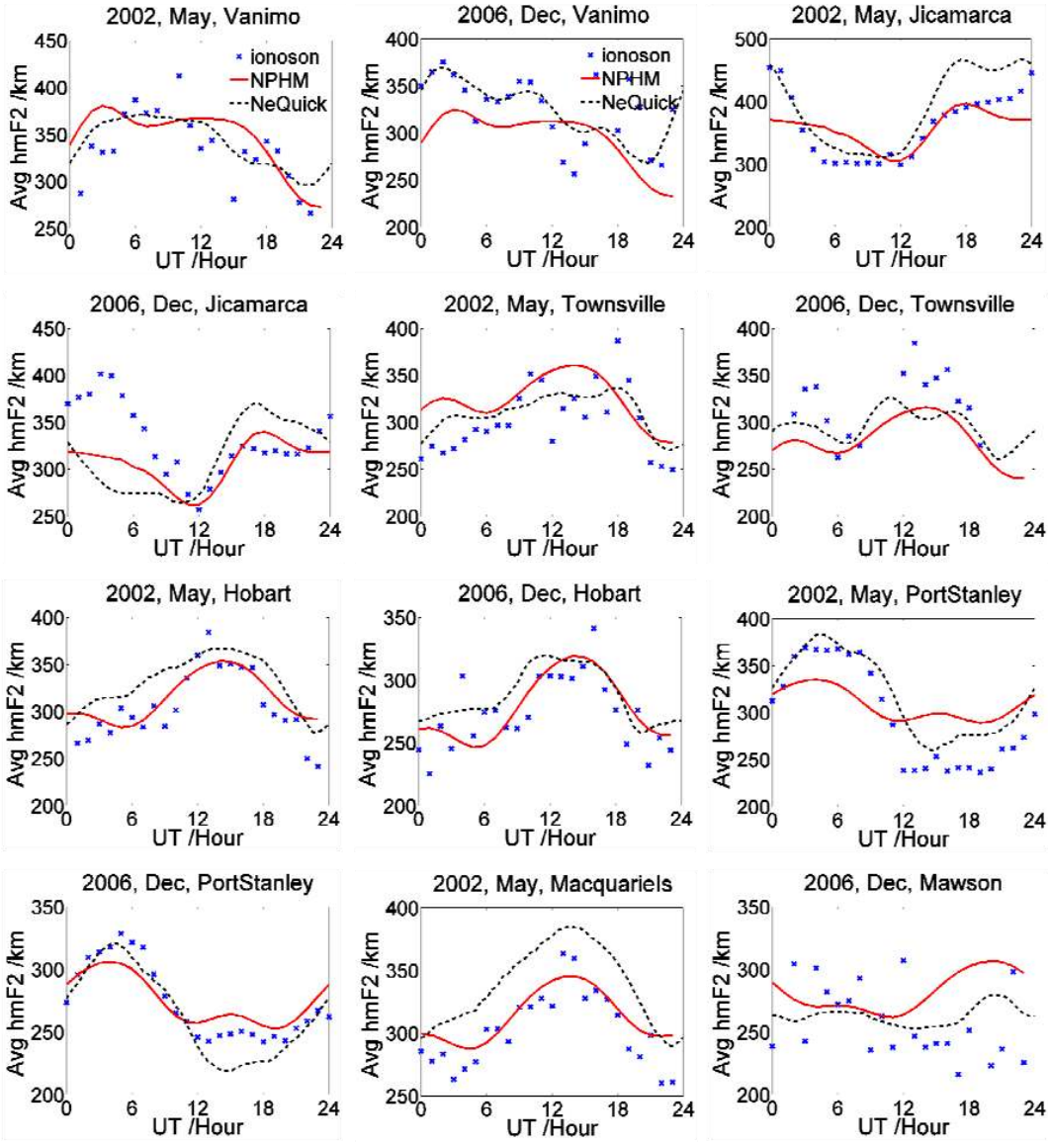

Fig. 8. Monthly mean of NPHM and NeQuick as a function of UT in comparison with ionosonde observation at Southern Hemisphere stations.

The solar radio flux index F10.7 is the main driving function of the proposed NPHM. However, the NPHM is climatological, i.e. it maps the long- time average behaviour of the peak density height. The small-scale features of the peak density height are smoothed out in the averaging and fitting procedures. It should be mentioned that an empirical model based on climatology cannot predict the actual variability and dynamics of the ionosphere. However, in operational ionospheric parameters reconstruction using real-time observations, the use of any empirical model as a background model is very helpful (see use of the background model for TEC reconstruction, Jakowski et al., 2011b).

Our comprehensive validation studies using CHAMP and COSMIC IRO observations and ionosonde measurements show that the performance of the new model is very similar to that of the NeQuick model. The NeQuick as well as the IRI use the CCIR M(3000)F2 maps for *hm*F2 estimations at any place and time. The IRI uses modified Bilitza et al. (1979) equations for M(3000)F2 conversion to *hm*F2 whereas the NeQuick model uses the algorithm given by Radicella and Zhang (1995) based on the Dudeney (1978, 1983) formula. In the present paper we did not compare our model with the IRI. However, since both the NeQuick and IRI use CCIR maps for *hm*F2 estimations, it is expected that comparisons with the IRI will be quite similar with those with the NeQuick model.

For global distribution of *hm*F2, our new model uses only 13 polynomial coefficients. Thus the number of coefficients

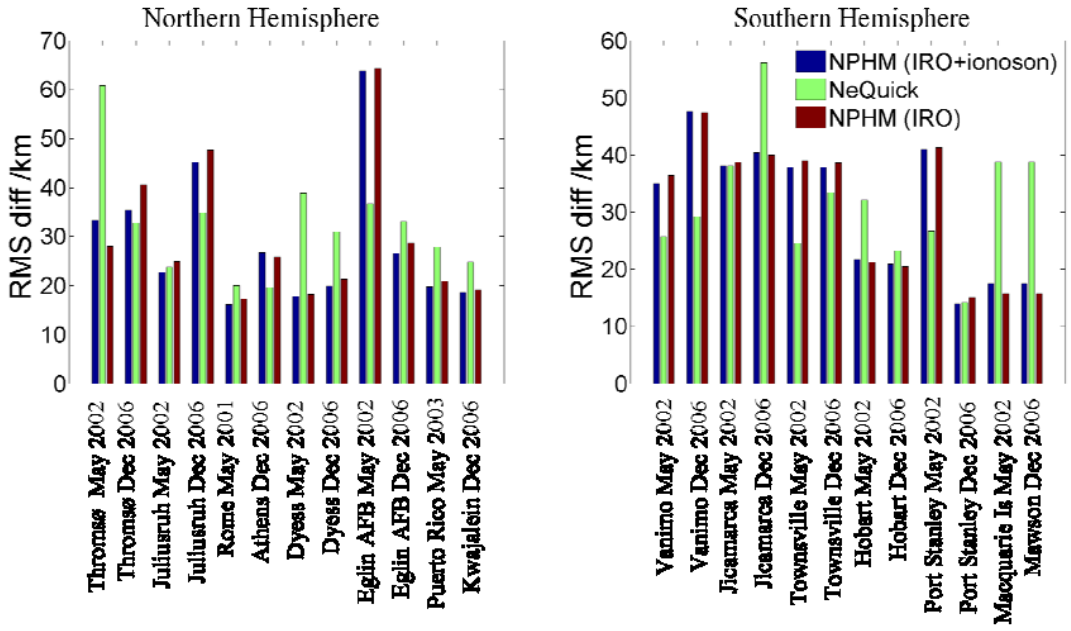

Fig. 9. Comparisons between NPHM (IRO+ionosonde and IRO solutions) and NeQuick model for RMS estimates of their differences from observational data.

Table 3. Geographic coordinates of the verification stations.

Verification stations	Geographic latitude/° N	Geographic longitude/° E	Validation period	
			May 2002	Dec 2006
Tromsø	69.7	19	√	√
Juliusruh	54.5	13.4	√	√
Rome	41.8	12.5	May 2001	–
Athens	38.0	23.5	–	√
Dyess AFB	32.4	−99.7	√	√
Eglin AFB	30.4	−86.7	√	√
Puerto Rico	18.5	−67.2	May 2003	–
Kwajalein	9.0	167.2	–	√
Vanimo	−2.7	141.3	√	√
Jicamarca	−12.1	−77	√	√
Townsville	−19.63	146.85	√	√
Hobart	−42.92	147.32	√	√
Port Stanley	−51.7	−57.8	√	√
Macquarie Island	−54.5	159.0	√	–
Mawson	−67.6	62.88	–	√

used by the new model is at least 2 orders of magnitude less than those used by the CCIR map. Therefore, the great benefit of the new model is the ease of implementation and use. Due to limited number of coefficients, both the computation time and power will be significantly reduced in real-time ionosphere monitoring or modelling using the new model. The new model can also be used as an alternative of the CCIR map within any 3-D ionosphere model.

6 Conclusions

We presented a global peak density height model NPHM, consisting of a set of nonlinear equations that explicitly describe the functional dependencies of *hm*F2 on local time, season, geographic/geomagnetic latitudes, and solar cycle variations. The NPHM approach contains 13 unknown polynomial coefficients in addition to a few empirically fixed known parameters. The polynomial coefficients are derived by applying the model approach to a vast quantity of global *hm*F2 data derived from radio occultation and ionosonde

measurements. Comparisons between NPHM and electron density NeQuick models for RMS estimates of their differences from observational data show that during high solar activity period the RMS deviations are about 13 % and 18 % for NPHM and NeQuick models, respectively. During low solar activity periods, the corresponding RMS estimates are 12 % and 16 %, respectively. The performance of the new model may be further improved in the future by extending the model database by integrating available topside sounder data and utilizing IRO data from upcoming satellite missions.

Acknowledgements. The authors would like to give thanks to sponsors and operators of the CHAMP and GRACE missions; Deutsches GeoForschungsZentrum (GFZ) Potsdam, German Aerospace Center (DLR), and the US National Aeronautics and Space Administration (NASA). The authors are grateful to sponsors and operators of the FORMOSAT-3/COSMIC mission; Taiwan's National Science Council and National Space Organization (NSPO), the US National Science Foundation (NSF), National Aeronautics and Space Administration (NASA), National Oceanic and Atmospheric Administration (NOAA) and the University Corporation for Atmospheric Research (UCAR). The authors are also grateful to the Australian Space Weather Agency for publishing ionosonde data via IPS radio and space services. The authors would like to give thanks to NGDC for disseminating historical ionosonde data via SPIDR. This research is essentially supported by the Ministry of Education and Science of Mecklenburg-Vorpommern under grant AU 07 008.

Topical Editor K. Kauristie thanks T. Jayachandran and another anonymous referee for their help in evaluating this paper.

References

Altinay, O., Tulunay, E., and Tulunay, Y.: Forecasting of ionospheric critical frequency using neural networks, Geophys, Res. Lett., 24, 1467–1470, 1997.

Angling, M. J.: First assimilations of COSMIC radio occultation data into the Electron Density Assimilative Model (EDAM), Ann. Geophys., 26, 353–359, doi:10.5194/angeo-26-353-2008, 2008.

Bilitza, D.: International reference ionosphere 2000, Radio Sci., 36, 261–275, doi:10.1029/2000RS002432, 2001.

Bilitza, D. and Reinisch, B. W.: International Reference Ionosphere 2007: Improvements and new parameters, Adv. Space Res., 42, 599–609, doi:10.1016/j.asr.2007.07.048, 2008.

Bilitza, D., Sheikh, N. M., and Eyfrig, R.: A global model for the height of the F2-peak using M3000 values from CCIR, Telecommun. J., 46, 549–553, 1979.

Bilitza, D., Rawer, K., Bossy, L., Kutiev, I., Oyama, K., Leitinger, R., and Kazimirovsky, E.: International Reference ionosphere 1990, Nat. Space Sci. Data Cent., Report 90-22, Greenbelt, Md, 1990.

Bradley, P. A. and Dudeney, J. R.: A simple model of the vertical distribution of electron concentration in the ionosphere, J. Atmos. Terr. Phys., 35, 2131–2146, 1973.

CCIR: Atlas of ionospheric characteristics, Comite' Consultatif International des Radiocommunications, Reports, 340, 340-2, later supllements, ITU, Geneva, 1967.

Coisson, P., Radicella, S. M., Leitinger, R., and Nava, B.: Topside electron density in IRI and NeQuick: Features and limitations, Adv. Space Res., 37, 937–942, 2006.

Dudeney, J. R.: An improved model of the variation of electron concentration with height in the ionosphere, J. Atmos. Terr. Phys., 40, 195–203, 1978.

Dudeney, J. R.: The accuracy of simple methods for determining the height of the maximum electron concentration of the F2-layer from scaled ionospheric characteristics, J. Atmos. Terr. Phys., 45, 629–640, doi:10.1016/S0021-9169(83)80080-4, 1983.

Fox, M. W. and McNamara, L. F.: Improved world-wide maps of monthly median of *fo*F2, J. Atmos. Terr. Phys., 50, 1077–1086, 1988.

Gulyaeva, T. L., Bradley, P. A., Stanislawska, I., and Juchnikowski, G.: Towards a new reference model of *hm*F2 for IRI, Adv. Space Res., 42, 666–672, doi:10.1016/j.asr.2008.02.021, 2008.

Hajj, G. A. and Romans, L. J.: Ionospheric electron density profiles obtained with the Global Positioning System: Results from the GPS/MET experiment, Radio Sci., 33, 175–190, 1998.

Hoque, M. M. and Jakowski, N.: Estimate of higher order ionospheric errors in GNSS positioning, Radio Sci., 43, RS5008, doi:10.1029/2007RS003817, 2008.

Hoque, M. M. and Jakowski, N.: Ionospheric bending correction for GNSS radio occultation signals, Radio Sci., 46, RS0D06, doi:10.1029/2010RS004583, 2011a.

Hoque, M. M. and Jakowski, N.: A new global empirical *Nm*F2 model for operational use in radio systems, Radio Sci., 46, RS6015, doi:10.1029/2011RS004807, 2011b.

ITU-R: Reference ionosphere characteristics, Recommendation, P.1239 (approved in 1997-05, managed by ITU-R Study Group SG3), 1997.

Jakowski, N., Wehrenpfennig, A., Heise, S., Reigber, C., and Lühr, H.: GPS Radio Occultation Measurements of the Ionosphere on CHAMP: Early Results, Geophys. Res. Let., 29, 1457, doi:10.1029/2001GL014364, 2002.

Jakowski, N., Leitinger, R., and Angling, M.: Radio occultation techniques for probing the ionosphere, Annals of Geophysics, 47, 1049–1066, 2004.

Jakowski, N., Hoque, M. M., and Mayer, C.: A new global TEC model for estimating transionospheric radio wave propagation errors, J. Geod., 85, 965–974, doi:10.1007/s00190-011-0455-1, 2011a.

Jakowski, N., Mayer, C., Hoque, M. M., and Wilken, V.: Total electron content models and their use in ionosphere monitoring, Radio Sci., 46, RS0D18, doi:10.1029/2010RS004620, 2011b.

Jones, W. B. and Gallet, R. M.: Representation of diurnal and geographic variations of ionospheric data by numerical methods, ITU Tele-communication Journal, 29, 129–149, 1962.

Jones, W. B. and Gallet, R. M.: Representation of diurnal and geographic variations of ionospheric data by numerical methods, ITU Tele-communication Journal, 32, 18–29, 1965.

Jones, W. B. and Obitts, D. L.: Global representation of annual and solar cycle variation of *fo*F2 monthly median 1954–1958, US Institute for Telecommunication Science, Research Report OT/ITSRR 3, National Technical Information Service, COM 75-11143/AS, Springfield, VA, 1970.

Kishcha, P. V. and Kochenova, N. A.: Model for the height of the ionosphere maximum in main ionospheric trough zone, Geomagn. Aeronomy, 36, 787–789, 1996.

Kumluca, A., Tulunay, E., and Topalli, I.: Temporal and spatial forecasting of ionospheric critical frequency using neural networks, Radio Sci., 34, 1497–1506, 1999.

Leitinger, R., Titheridge, J. E., Kirchengast, G., and Rothleitner, W.: A "simple" global empirical model for the F layer of the ionosphere, Wissenschaftliche Berichte 1/1995, IMG, University of Graz, 1995.

Liu, C., Zhang, M.-L., Wan, W., Liu, L., and Ning, B.: Modeling M(3000)F2 based on empirical orthogonal function analysis method, Radio Sci., 43, RS1003, doi:10.1029/2007RS003694, 2008.

Mandea, M. and Macmillan, S.: International Geomagnetic Reference Field – the eighth generation, Earth Planets Space, 52, 1119–1124, 2000.

McKinnell, L. A. and Poole, A. W. V.: Ionospheric variability and electron density profile studies with neural networks, Adv. Space Res., 27, 83–90, 2001.

McNamara, L. F., Reinisch, B. W., and Tang, J. S.: Values of *hm*F2 deduced from automatically scaled ionograms, Adv. Space Res., 7, 53–56, 1987.

Nava, B., Coisson, P., and Radicella, S. M.: A new version of the NeQuick ionosphere electron density model, J. Atmos. Solar Terr. Phys., 70, 1856–1862, doi:10.1016/j.jastp.2008.01.015, 2008.

Oyeyemi, E. O. and Poole, A. W. V.: Towards the development of a new global *fo*F2 empirical model using neural networks, Adv. Space Res., 34, 1966–1972, 2004.

Oyeyemi, E. O., Poole, A. W. V., and McKinnell, L. A.: On the global model for *fo*F2 using neural networks, Radio Sci., 40, RS6011, doi:10.1029/2004RS003223, 2005.

Piggott, W. R. and Rawer, K.: U.R.S.I. Handbook of Ionogram Interpretation and Reduction, US Department of Commerce, National Oceanic and Atmospheric Administration, Environmental Data Service, Asheville, NC, USA, 325 pp., 1972.

Piggott, W. R. and Rawer, K.: U.R.S.I. Handbook of Ionogram Interpretation and Reduction, second ed., World Data Center A for Solar-Terrestrial Physics, Report UAG-23A, 1978.

Poole, A. W. V. and Poole, M.: Long-term trends in *fo*F2 over Grahamstown using neural networks, Ann. Geophys., 45, 155–161, 2002.

Radicella, S. M. and Leitinger, R.: The evolution of the DGR approach to model electron density profiles, Adv. Space Res., 27, 35–40, doi:10.1016/S0273-1177(00)00138-1, 2001.

Radicella, S. M. and Zhang, M. L.: The improved DGR analytical model of electron density height profile and total electron content in the ionosphere, Annali di Geofisica, XXXVIII, 35–41, 1995.

Rush, C. M., Pokempner, M., Anderson, S. F. G., and Perry, J.: Improving ionospheric maps using theoretically derived values of *fo*F2, Radio Sci., 18, 95–107, 1983.

Rush, C. M., Pokempner, M., Anderson, D. N., Stewart, F. G., and Perry, J.: Maps of *fo*F2 derived from observations and theoretical data, Radio Sci., 19, 1083–1097, 1984.

Shimazaki, T.: World daily variability in the height of the maximum electron density of the ionospheric F2-layer, J. Radio Res. Lab. (Japan), 2, 85–97, 1955.

Titheridge, J. E.: Re-modeling the ionospheric E region. Kleinheubacher Berichte, 39, 687–696, 1996.

Tulunay, E., Özkaptan, C., and Tulunay, Y.: Temporal and spatial forecasting of the *fo*F2 values up to twenty four hours in advance, Phys. Chem. Earth(c), 25, 281–285, 2000.

Wintoft, P. and Cander, L. J. R.: Short-term prediction of *fo*F2 using time delay neural networks, Phys. Chem. Earth(c), 24, 343–347, 1999.

Xenos, T. D.: Neural-network-based prediction techniques for single station modeling and regional mapping of the *fo*F2 and M(3000)F2 ionospheric characteristics, Nonlin. Processes Geophys., 9, 477–486, doi:10.5194/npg-9-477-2002, 2002.

Yue, X., Schreiner, W. S., Lei, J., Sokolovskiy, S. V., Rocken, C., Hunt, D. C., and Kuo, Y.-H.: Error analysis of Abel retrieved electron density profiles from radio occultation measurements, Ann. Geophys., 28, 217–222, doi:10.5194/angeo-28-217-2010, 2010.

Zhang, S.-R., Oliver, W. L., Holt, J. M., and Fukao, S.: Ionospheric data assimilation: comparison of extracted parameters using full density profiles and key parameters, J. Geophys. Res., 108, 1131, doi:10.1029/2002JA009521, 2003.

Zhang, M.-L., Liu, C., Wan, W., Liu, L., and Ning, B.: A global model of the ionospheric F2 peak height based on EOF analysis, Ann. Geophys., 27, 3203–3212, doi:10.5194/angeo-27-3203-2009, 2009.